Journal of King Saud University – Science 35 (2023) 102856

HOSTED BY

Contents lists available at ScienceDirect

Journal of King Saud University – Science

journal homepage: www.sciencedirect.com

Original article

Synthesis, characterization of vanadium oxide nanostructures and their cytotoxic activities in human cell lines

Javed Ahmad [a,*], Rizwan Wahab [a], Maqsood A. Siddiqui [a], Quaiser Saquib [a], Abdulaziz A. Al-Khedhairy [a]

[a] Chair for DNA Research, Zoology Department, College of Science, King Saud University, Riyadh 11451, Saudi Arabia

ARTICLE INFO

Article history:
Received 16 May 2023
Revised 22 June 2023
Accepted 14 August 2023
Available online 20 August 2023

Keywords:
Vanadium pentaoxide
SEM
MTT
NRU
ROS
MCF-7 cell line

ABSTRACT

Vanadium oxide is largely applied as a chemical and industrial product in various field such as in electrochemical, photochemical and refining industries. Very limited studies are available for the use of vanadium oxide to understand the biological activity against cancer cells. The work presented here, to understand the cytotoxicity study against breast cancer cells (MCF-7). Initially, vanadium penta oxide (V_2O_5) nanorods were synthesized via solution process and were well characterized. The size of the crystallite, phase and morphology of the powder were scrutinized via X-ray diffraction (XRD), field emission scanning electron microscope (FESEM) respectively. The size of each rod shaped structure is ~2–3 μm length whereas diameter goes 200–250 nm. The cytotoxicity study with this structure has not been studied previously. Therefore, the current work carried out to investigate the efficacy against cancer cells. The cells cytotoxic assesement were analysed via MTT((3-[4,5-dimethylthiazol-2-yl]-2,5 diphenyl tetrazolium bromide) and NRU (Neutral Red Uptake) assays with varied V_2O_5 concentrations (2–200 μg/m L), which indicates the reduction in cell viability. The reactive oxygen species (ROS) were measured in cancer cells as the concentration of V_2O_5 increases, the ROS is increase in the cells, which is the indication of cells death. Also, the RT-PCR study revealed that the mRNA levels of apoptotic genes such as p53, bax, and caspase-3 were up regulated, whereas bcl-2, an anti-apoptotic gene, was down regulated with the interaction of V_2O_5 increases.

1. Introduction

Vanadium is an attractive metal for the chemists, biologists, biochemists, toxicologists, and pharmacologists. Due to many inorganic and orgnic complexes form, this material is essential for the treatment of certain diseases in humans (Nriagu, 1998, Tracey et al., 2007). Vanadium exist with different oxidation states +2, +3, +4, and +5 and the most commonly in the tetravalent and pentavalent form (Imtiaz et al., 2015). Its largely utilized in industries as glass, paint, ceramic, photographic, chemical, electrochemical, etc. Vanadium is also used in metallurgical industry for the production of steel and non-ferrous alloys (Fortoul and Rojas-Lemus, 2007). Apart from the physical and chemical characteristics, vanadium pentoxide (V_2O_5) utilized to explore the biological activity and it depends upon number of factors for instance, their derivative type, doses, administration, treatment period etc. Also, the different oxidation states relies to their concentrations, pH, annealing or pretreatment conditions of vanadium (Gill et al., 2010).

Its estimated that nearly 85% of V_2O_5 is utilized as an intermediate for the production of ferrovanadium alloy, which is used to produce high strength low alloy steels (Lagneborg et al., 1999) also used ~10% for production of alloys of titanium (Veiga et al., 2012). Due to the variable oxidation states of V_2O_5, its used as as a catalyst for the conversion of in sulfur dioxide (SO_2) to sulfur trioxide (SO_3) to produce sulphuric acid (Asher and Golwalkar, 2013), also prepration of acid anhydrides such as maleic anhydride from butane (Tedder, 1975). A larger industrial utalities of V_2O_5, it also usese as a pigment in ceramics (ATSDR, 2012), primarily metalloporphyrins which are present in coal and oils (Dechaine and Gray, 2010).

* Corresponding author at: Zoology Department, College of Science King Saud University, Riyadh 11451, Saudi Arabia.
E-mail address: javedahmad@ksu.edu.sa (J. Ahmad).

Peer review under responsibility of King Saud University.

Production and hosting by Elsevier

https://doi.org/10.1016/j.jksus.2023.102856

In case of biological applications, vanadium produces the reactive oxygen species (ROS) in cells and it resulted the reduction of vanadate to vanadyl (Aureliano and Gândara, 2005). The traces of vanadium can have the capability to from oil combustion and that are found throughout the environment and for some biological systems considered its an essential trace element (Dai et al., 2016, Zhang et al., 2001). The environment is also affected the increase of vanadium level in atmosphere that is due to the upsurge rate of fuel combustion with enhance vanadium content. (Calderon-Garcidueñas, et al., 2002, Fortoul, et al., 2002, Gutierrez-Castillo, et al., 2006).

The vanadium affects to the respiratory system and it creates the inconsequential action on the gastrointestinal system due to the less gut absorption rate of the substance (Ress, et al., 2003). The V_2O_5 affect as toxic and carcinogenic compound in the environment, also affect to the NK cells immune response system and it increased the PTEN and decreased SHP1 expression through dysregulating interleukin (IL)-2/IL-2R-mediated JAK signaling pathways with inducing apoptosis (Gallardo-Vera, et al., 2018). The V_2O_5 could inhibit, the proliferation of NK-92MI cells as well as their secretion of anti-inflammatory IL-10 cytokine and proinflammatory IFNγ (Gallardo-Vera et al., 2016).

The purpose of this work is to investigate the effect of V_2O_5 on breast cancer cells because it is common cancer worldwide and affected the female candidate especially. Due to these reasons, we have selected the breast cancer cell lines MCF-7 to check the cytological study with vanadium pentoxide, used frequently in industries. Initially, the material was synthesized via solution process and analysed with instruments such as X-ray diffraction pattern, FESEM (field emission scanning electron microscopy), FTIR (fourier transform infrared spectroscopy), UV–vis (UV–visible spectroscopy) and TGA (Thermo grivimetric analysis) respectively. The cells morphology was examined via microscopy, whereas the cytotoxicity tests were measured to know the cells viability via MTT and NRU assays. The ROS generation and RT-PCR (reverse transcription-polymerase chain reaction) studies were also conducted to know the effect of cancer cells at different concentrations. Based on the results and their analysis a possible discussion was also explained here.

2. Materials and methods

2.1. Materials used for synthesis of V_2O_5

For the preparation of V_2O_5 nanorods, sodium hydroxide (NaOH), ammonium meta vanadate (NH_4 VO_3), oxalic acid were purchased from Aldrich chemical corporation, U.S.A and used without any further purifications.

2.2. Synthesis of V_2O_5 nanorods

The synthesis of V_2O_5 nanorods (V_2O_5NRs) were accomplished via co-precipitation solution method as followed the previously published literature (Govindarajan et al.2019) with minor modification. For the synthesis of V_2O_5NRs, initially, the oxalic acid (0.3 M) was dissolved in 100 ml of distilled water under magnetic stirring at 60 °C for ~30 min. Thereafter, to this solution, ~5 g of ammonium metavanadate (NH_4VO_3) and sodium hydroxide (0.2 M) were added slowly and mix well into the oxalic acid solution. At this time, the white colored solution changes into the greenish blue color, which indicates the formation of V_2O_5. The solution was transferred to the refluxing pot and heated at 90 °C for 6 h and final green colored product was recovered via alcohol washing.

2.3. Characterization

The size of the nanocrystals, crystallinity and phases of the prepared powder was determined by using X-ray powder diffractometer (XRD) $Cu_{K\alpha}$ radiation (λ = 1.54178 Å, PANalytical XPert Pro, U.S.A.) with Bragg angle ranging from 10° to 80° with 6°/min scanning speed. The morphology of the product was analyzed with using FESEM (Jeol, JSM, Japan) as described previously (Wahab et al., 2022a). Also the FTIR (Perkin Elmer-FTIR Spectrum-100, U.S.A) spectroscopy was analyzed in the range of 400–4000 cm^{-1}. The UV–visible spectroscopy (V-770, UV–Visible spectrophotometer, Jasco, U.S.A) was used from the range of 300–800 nm with the baseline correction. The thermal stability test in terms of thermal gravimetric analysis (TGA, Mettler Toledo AG, Analytical CH-8603, Schwerzenbach, Switzerland) was also conducted. For this experiment ~ 5.8 mg of powder was loaded into alumina crucibles (Al_2O_3) and heated till to 800 °C with a heating ramp of 20 °C/min under nitrogen gas with a flow of 20 ml/min.

2.4. Cell culture

The cancer cell lines (Breast cancer (MCF-7) cells) were purchased from the American Tissue culture and collection (ATCC, USA) were cultured in DMEM-F12 supplemented with 10% fetal bovine serum, 100 U/mL penicillin, and 100 μg/mL streptomycin at 37 °C in a humidified 5% CO_2 incubator and cells were passaged at every alternate days.

2.5. Cell viability assays

MTT assay, which is also known with the chemical compound (3-(4, 5-dimethylthiazolyl-2)-2, 5-diphenyltetrazolium bromide) was carried out as according to the previously protocol described by Mosmann (Mosmann 1983) with some modifications. About 15,000–20,000 cells were cultured in a specialized 96-well plate. The treatment with prepared nanostructured product was accomplished at the cells confluence reached to 80–90%. Once the cells were exposed well (after 24 h) with the prepared nanostructures product, the MTT assay was measured in term of absorbance at 570 nm with a plate reader (Synergy HT).

The cytotoxicity of the prepared V_2O_5 was also checked via NRU assay. The cells were initially grown in 96 well plates for 24 h. Thereafter, the cells were exposed with nanostructures concentration (2–200 μg/mL) and to kept in an incubator for 24 h. After the exposure, cells were further incubated in NR medium for 3 h and then cells were washed and extracted in 1% acetic acid and 50% ethanol and analyzed at 540 nm.

2.6. Mitochondrial membrane potentials analysis

Mitochondrial membrane potentials (MMP) was measured as described by Zhang, et al., 2011 for both treated and untreated cells exposed with MCF-7 cells. Briefly, MCF-7 cells were exposed to 25 μg/mL to 200 μg/mL Venedium penta oxide for 24 h. Thereafter, both treated and untreated cells were washed two to three times with PBS and subsequently treated with fluorescent dye 10 μg/mL Rh 123, for 1 h at 37 °C in the dark conditions. The fluorescence was measured using a (OLYM -PUS CKX 41) fluorescence microscope.

2.7. Reactive oxygen species (ROS) generation

The ROS was tested by using 2, 7-dichloro di hydrofluoresce in diacetate (DCFH-DA; Sigma Aldrich, USA) dye, which is utilized as a fluorescent agent and followed the protocol as described earlier (Zhang et al., 2001). The cells were exposed with the processed

material for 24 h, and washed well twice with PBS and incubated for 30 min in DCFH-DA (20 μM) in dark medium at 37 °C. Once the reaction of DCFH-DA with control and treated cells were completed, it was analyzed with intracellular fluorescence using fluorescence microscope.

2.8. Gene expression study

Total RNA was purified from 3 × 10^5 cells/well of MCF-7 cells untreated and treated with V_2O_5 NRs (100 μg/ml) for 24 h using the RNeasy mini Kit (Qiagen) as per the manufacturer's protocol.

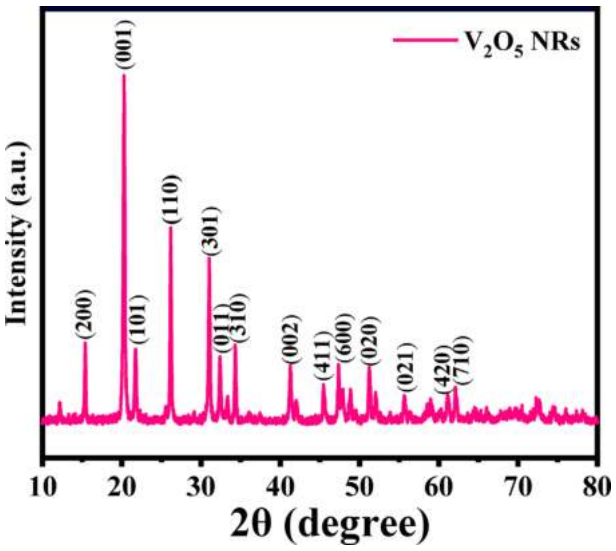

Fig. 1. X-ray diffraction pattern of V_2O_5NRs.

The RNA concentration were analysed by using Nanodrop 8000 spectrophotometer (Thermo Scientific, USA) and the integrity of RNA was confirmed by 2% agarose gel using the documentation system (Universal Hood II, BioRad, USA). The complimentary DNA was made by the MLV reverse transcriptase (GE Health Care, UK) kit according to the protocol instruction taking 2 μg of total RNA and 100 ng of oligo (dT)12–18 primer. For the quantification of apoptotic and anti-apoptotic gene a set of primers was used for the determination of gene expression. Following the recommended cycling program using Roche® LightCycler®480 (96-well block), the reaction mixture of 20 μl taking 100 ng of the cDNA and 7.5 μM of each primer with 2 × of SYBR Green I Roche Diagnostics. The cycling conditions at 95 °C for 10 min denaturation step, followed by 40 cycles of 95 °C for 15*s* denaturation, 60 °C for 20*s* annealing, and 72 °C for 20*s* elongation steps. Expressed genes data were analyzed by GAPDH, as an internal housekeeping control gene.

3. Results

3.1. X-ray diffraction (XRD) analysis

The powder product was analyzed with XRD for to understand the crystallite size, phases and d-spacing of the material. The spectrum reveals number of peaks at different peaks positions with their phases such as 15.4 <200>, 20.28 <100>, 21.74 <101>, 26.2 <110>, 31.08 <301>, 32.38 <011>, 34.3 <310>, 41.28 <002>, 45.54 <411>, 47.38 <600>, 51.22 <020>, 55.64 <021>, 61.22 <420> and 62.08 <710> (Fig. 1). These assigned peaks in the XRD pattern are having orthorhombic structure and are matched well with JCPSD card no. V_2O_5 (JCPDS # 022–25590813, lattice parameters a = 11.51 Å, b = 3.56 Å and c = 4.37Å. The growth direction towards [001] direction and intense and sharp peaks attributed that the prepared material is highly crystalline in nature (Govindarajan et al., 2019). The crystallite size of V_2O_5 was calculated with using

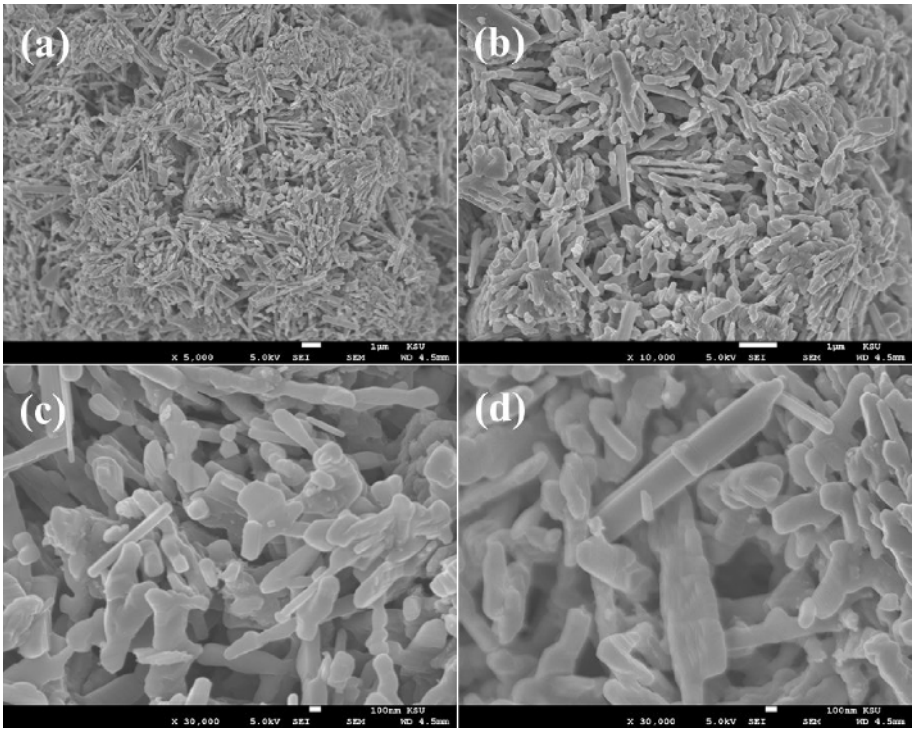

Fig. 2. SEM images of V_2O_5NRs; (a-b) represent the rod shaped structure captured at low magnification whereas (c-d) show the rods shaped structures with an individual size (L = 2–3 μm and D=∼200–250 nm) captured at high magnification scale.

Scherrer's formula as described previously (Wahab et al., 2022a) and its shows that the average particle size was ~ 16.3 nm (Fig. 1).*3.2. Morphological observations (FESEM result)*

The FESEM was utilized to know the morphology of the prepared powder product, as described in material and method, and the obtained pictures are shown as Fig. 2a-d. To observe in detailed morphological examination of the prepared product, a low and high-scale magnification scale pictures were recorded, which shows the rod shaped morphology. In Fig. 1(a), it can be easily seen that the produced powder have nanorods (NRs) with tetragonal and smooth surface shaped structures. The average length and diameter of formed individual NR is in the range of 2–3 μm (Fig. 2a and b), whereas the diameter varies from 200 to 250 nm. The NR surfaces are clear and smooth and orthorhombic crystallite structure in shape, which is a typical characteristic of V_2O_5 (Fig. 2c). From the close observation of the FESEM pictures, it seems that the individual NR to be a petal of flower morphology that's originated from a center point with length of an individual rod/petal varies from 2–3 μm (Fig. 2d).

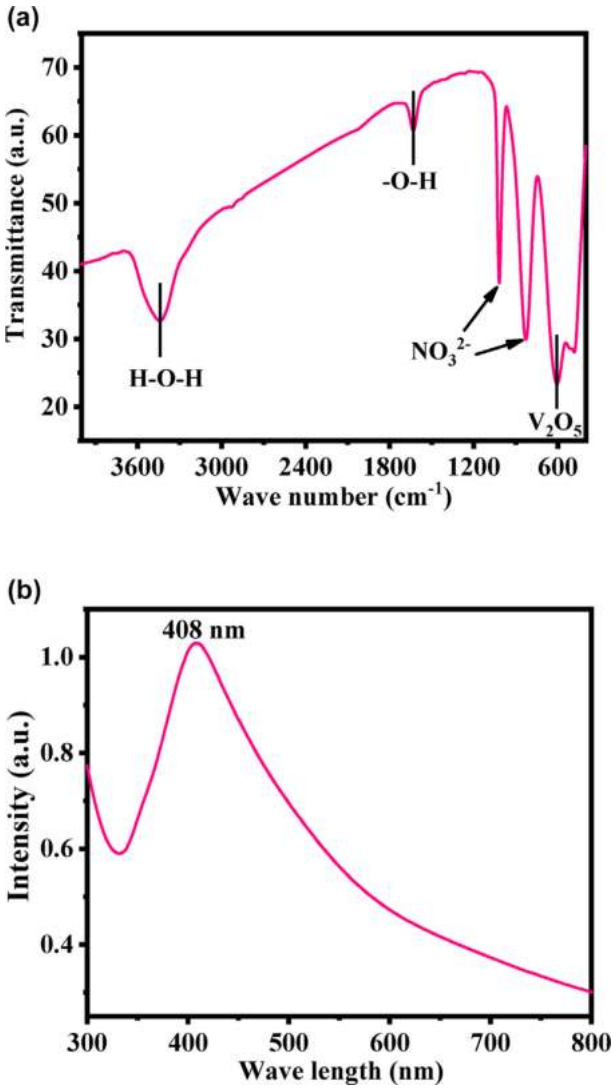

Fig. 3. (a). FTIR spectroscopy of V_2O_5NRs, which represent the functional groups presents in the product whereas **(b)** shows the UV–visible spectroscopy of V_2O_5NRs.

3.3. Functional groups analysis (FTIR results)

The functional groups in the prepared powder was examined and assigned the FTIR spectroscopy and represent as Fig. 3a. The peak at 610 cm^{-1} is related to V_2O_5 whereas the bands at 3200–3600 cm^{-1} correspond to O—H mode of vibration. The small asymmetric stretching mode of vibration of O—H was observed between 1628 cm^{-1}. The symmetric and asymmetric stretching vibrational peak occurs between 1018 and 830 cm^{-1} which designates the vibration of NO_3^1 ions (Vijayakumar et al., 2015).

3.4. Optical analysis (UV–visible spectroscopy results)

The optical property of the product was also examined with UV–visible spectroscopy. A shallow peak was detected in the spectrum at 408 nm (band gap ~ 3.039 eV) (Fig. 3b), which is a characteristic peak for V_2O_5. The band gaps express that material is much efficient and optically active, exhibit good chemical and optical characteristic (Vijayakumar et al., 2015).

3.5. Thermogravimetric analysis (TGA results)

Thermogravimetric analysis (TGA) is a technique via % mass loss was determined with increasing the temperature. The obtained TGA data (Fig. 4a) shows the prepared powder samples exhibits two-step of weight loss, one is solvent evaporation whereas another one is the powder stability/stabilization phase respectively. In this experiment, the initial step, which is solvent vaporization phase starts at 313 °C and completed at 655 °C with a weight loss of 3.31%. Thereafter, the secondary weight loss starts at 680 °C, which is also knows as burning or chemical decomposition phase, completed at 900 °C with a total weight loss was 18.52%. This phase illustrates the stabilization phase of prepared V_2O_5 and from these observation its shows that very less amount was loosed (Dey et al., 2019). In this experiment, it's observed that the total weight loss was calculated from 25 °C to 900 °C was 18.52%. The obtained data reveals that the material is highly stable at higher temperatures and are analogous with other studies (XRD and FTIR).

3.6. Microscopic results for cells morphology

The general morphology of the cultured cancer cells and treated with V_2O_5NRs were examined via microscopic study at 24 h incubation periods with a increasing concentrations (2 to 200 μg/ mL) ranges of V_2O_5NRs (Fig. 4b). The cultured cells morphology was used as a control whereas treated images were captured at different concentrations of NRs respectively (Fig. 4b). The initial information observed from the images revels that the cells were nucleated and once the time of incubation period increase, their confluence was reached to their optimum level (~70–80 %,). At this level of confluence, the NRs were exposed with different concentrations (2 to 200 μg/mL) and examined. The observation stated that at initial concentration (25 μg/mL) there is no noteworthy change was seen, but once the concentration of NRs was increased to 50 to 200 μg/mL, the growth of cells was much affected. The microscopic images authenticated that the cells were damaged with the incorporation of V_2O_5NRs.

3.7. MTT assay

The cytotoxicity was examined with MTT assay with V_2O_5NRs. The MTT assay was calculated as described above with using

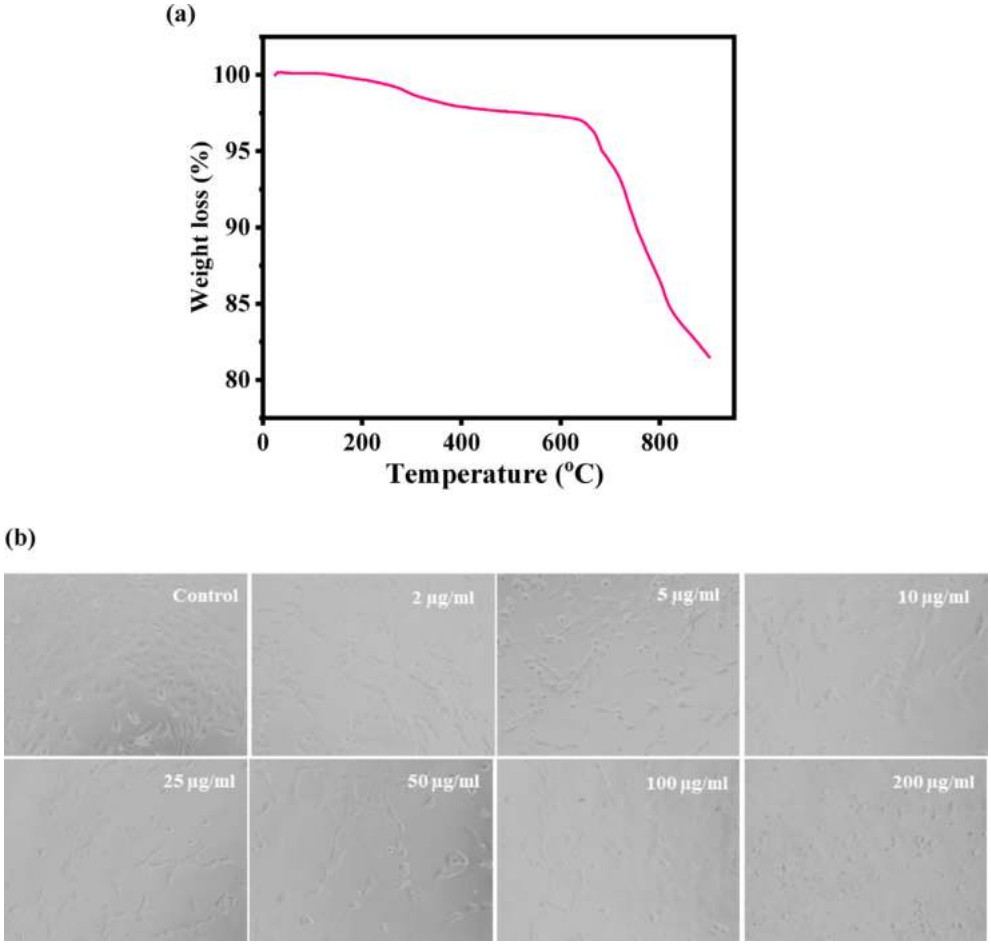

Fig. 4. (a). Thermogravimetric analysis (TGA) of V_2O_5NRs, and Fig. 4**(b)** shows the V_2O_5NRs-induced morphological changes in MCF-7 cells. Cells were exposed to V_2O_5NRs at various concentrations for 24 h. Images were taken using phase contrast inverted microscope at 20 × magnifications.

control and treated cancer cells, exposed in a range of different concentrations from 1 to 200 µg/ml for a period of 24 h incubation. The obtained data reveals that the viability of cancer cells were diminished with the incorporation of V_2O_5NRs and these data's showed concentration/dose-dependent manner. The MCF-7 cells viability, was decreases at 24 h 100%, 92%, 79%, 72%, 59%, 48% and 35% (Fig. 5) for the concentrations of 2, 5, 10, 25, 50, 100 and 200 µg/mL correspondingly ($p < 0.05$ for each). The data's shows that the cells viability was not much affected with initial concentration of the prepared nanostructures, whereas once the concentrations of the NRs exceeded to their optimum level, the cytotoxicity was much influenced.

3.8. NRU assay

The cytotoxicity was studied via NRU assay with V_2O_5NRs. The result was calculated using control and treated cells with concentrations 2–200 µg/ml. The NRU assay was decreases at 24 h 98%, 89%, 72%, 60%, 49%, 42% and 28% (Fig. 6) for the concentrations of 2, 5, 10, 25, 50, 100 and 200 µg/mL correspondingly

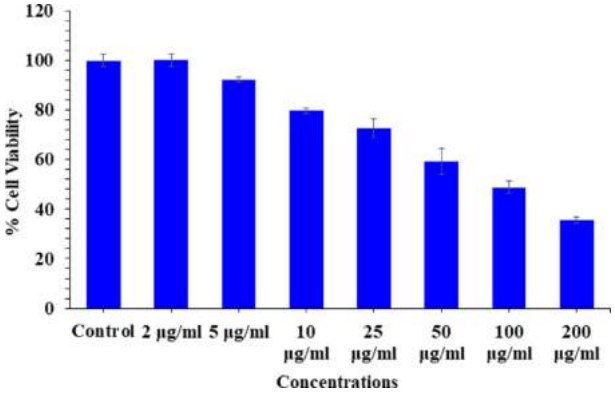

Fig. 5. Cytotoxic assessment of V_2O_5NRs in MCF-7 cells by MTT assay. Cells were exposed to various concentrations of V_2O_5NRs for 24 h.

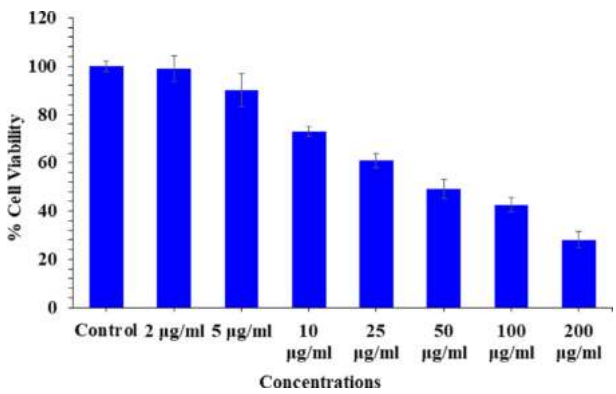

Fig. 6. Cytotoxic assessment of V_2O_5NRs in MCF-7 cells by NRU assay. Cells were exposed to various concentrations of V_2O_5NRs for 24 h.

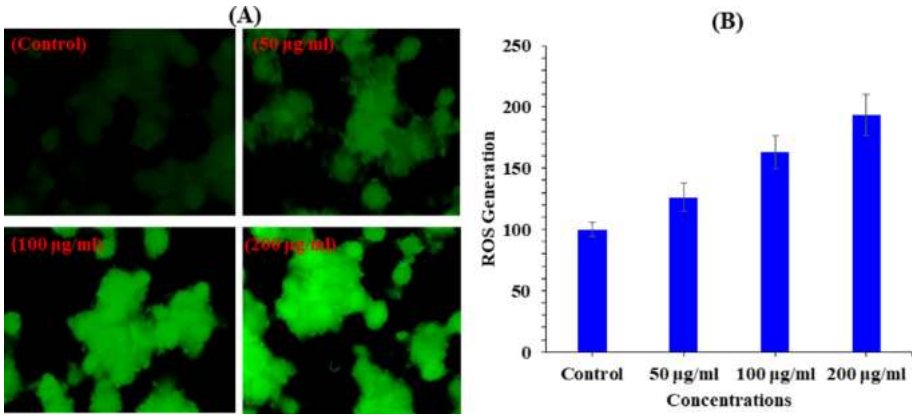

Fig. 7. V_2O_5NRs-induced ROS generation in MCF-7 cells after 24 h exposure. (A) Green fluore scence images showing the ROS generation in treated and untreated cells. (B) Percentage change in ROS generation in MCF-7 cells exposed to 2–200 µg/ml of V_2O_5NRs.

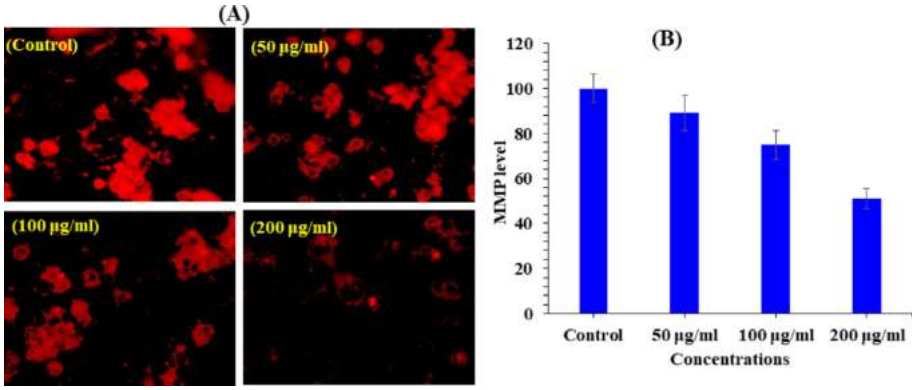

Fig. 8. V_2O_5NRs-induced MMP level in MCF-7 cells after 24 h exposure. (A) Fluorescence images showing MMP level in treated and untreated cells. (B) Percentage change in MMP level in MCF-7 cells exposed to 50,100 and 200 µg/ml of V_2O_5NRs. The graph is showing the percent induction in the ROS as compare to control group.

($p < 0.05$ for each). The data's shows that the cells viability was not much influenced with initial concentration of the NRs, whereas as the concentrations of the NRs exceeded the cytotoxicity was much influenced.

3.9. Generation of reactive oxygen species (ROS) induced cells with V_2O_5NRs

ROS generation was studied in MCF-7 cells after the exposure of V_2O_5NRs at a range of concentration 50, 100, and 200 µg/ml for a period of 24 h (Fig. 7A) with compared to control. ROS levels increased as the concentration of V_2O_5NRs rise. The ROS were rise at 50, 100 and 200 µg/ml were 126, 162, 193% as compared to control (100%) (Fig. 7B). Data represented are mean ± SD of three identical experiments in triplicates.

3.10. Analysis of Mitochondrial membrane potential (MMP) induced by V_2O_5NRs

MMP level was determined with V_2O_5NRs in MCF-7 cells exposed at a concentrations of 50, 100, and 200 µg/ml for a period of 24 h in Fig. 8A and B. The reduction of MMP level was noted in terms of fluorescence intensity of mitochondria specific dye Rh 123 (Fig. 8A). As shown in Fig. 8B. V_2O_5 decreased the fluorescence intensity of Rh 123. This reduction of MMP levels in MCF-7 cells treated with V_2O_5 NRs shows a significant decrease at three different concentrations 50, 100, and 200 µg/ml were 89, 75 and 51 respectively.

3.11. Quantification of apoptotic gene level by RT-PCR

The quantitative RT-PCR study was performed to check the mRNA level in MCF-7 cancer cells treated with V_2O_5NRs for 24 h at a concentration of 100 µg/ml. A number of marker genes were selected such as genes (p53, bax, casp3, and bcl-2) of the evaluation of mRNA level in cancer cells. Ominously altered the regulation of apoptotic genes in MCF-7 cells ($p < 0.05$ for each gene).

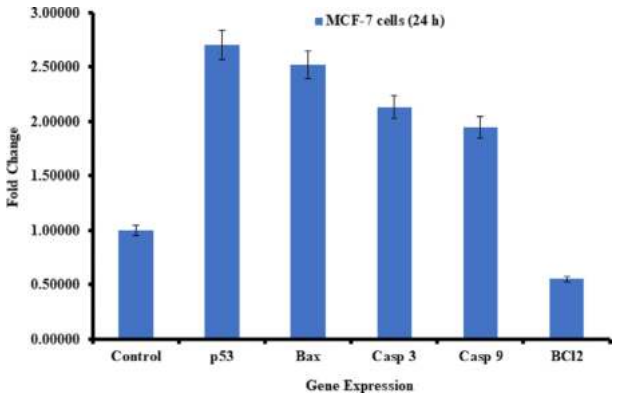

Fig. 9. Quantification of mRNA fold change, apoptotic genes (p53, bax, and casp3) and anti-apoptotic gene (bcl-2) was evaluated. MCF-7 cells treated 100 µg/mL of V_2O_5NRs for 24 h. Data obtained are mean ± SD of three experiments in triplicates ($p < 0.05$).

Obtained data shows that the mRNA levels of tumor suppresser of p53 gene (2.7) and the pro-apoptotic gene bax (2.5) were upregulated. Also identified that the expression level of caspase-3 (2.1) and caspase-9 (1.9) gene in V_2O_5NRs treated cells with control. The expression of bcl-2 (0.5), an anti-apoptotic gene was down regulated in cells treated with V_2O_5NRs (Fig. 9).

4. Discussion

Including the basic analysis of the prepared product, the core objective of the present study was to examine the cytotoxic responses of V_2O_5NRs with MCF-7 cancer cells. For this, the MTT and NRU assays shows the cytotoxicity against cancer cells with NRs at 2, 5, 10, 25, 50, 100 and 200 μg/mL concentrations for 24 h and shows that the viability of cells were in concentration/dose dependent and analogous to previously published literature (Ahmad et al., 2021). its believe that the cytotoxicity depends upon a number of factors such as cancer cells activity, nanostructures geometry, characteristic property, concentrations of the media, functions of the material are well responsible for the cell death (Wahab et al., 2022b). The ROS was also measured, which played a key role in cytological measurement. The ROS was measured after 24 h exposure of cancer cells with NRs. It's hypothesize the NRs/any foreign material exhibit the tendency to produce ROS in cells and are responsible for the toxicological effects. The cells organelles structures such DNA, protein, and lipids and their mechanism are much affected also their functions were affected with ROS generation and may responsible to cell death (Montiel-Dávalos et al., 2012). The study presented here, showed that V_2O_5NRs motivates the ROS generation in a specified doses in MCF-7 cells and due to that reason the cell cytotoxicity happens. It is summarizes that damage of cells organelles was influenced with interaction of V_2O_5NRs, and it resulted the increase of ROS generation, once treated with NRs. As per the obtained data's for instance X-ray diffraction pattern, morphological analysis (FESEM) and cytological study conducted via MTT, NRU assays, also ROS generation it may postulates that the toxicity in cells are dependent with V_2O_5NRs in a dose dependent manner with an organized way against the cancer cells not to destroyed barely.

5. Conclusions

The summary of current work shows that vanadium penta oxide nanorods (V_2O_5) were prepared and characterized. V_2O_5NRs were utilized against breast cancer cells (MCF-7) at different concentrations. The cells morphology was studied via inverted microscopy and it reveals that different concentrations of nanorods of V_2O_5 express a sequential cytological effect on cancer cells. The MTT and NRU assays were measured the viability of cells and the results clearly showed that at initial doses V_2O_5 doesn't show any change in the cells growth, whereas once the doses were increased the viability of the cells were much influenced. The ROS generation analysis also in consistent with the MTT and NRUs data and shows the V_2O_5 nanorods are effective against breast cancer cells. Also the gene expression study with marker genes (P53, caspase-3, Bax, Bcl2) reveals that apoptosis happens in breast cancer cells with nanorods of V_2O_5.

Declaration of Competing Interest

The authors declare that they have no known competing financial interests or personal relationships that could have appeared to influence the work reported in this paper.

Acknowledgements

The authors extend their appreciation to the Deputyship for Research & Innovation, Ministry of Education in Saudi Arabia for funding this research. (IFKSURC-1-3206)

Appendix A. Supplementary material

Supplementary data to this article can be found online at https://doi.org/10.1016/j.jksus.2023.102856.

References

Ahmad, J., Wahab, R., Akhtar, M.J., Ahmad, M., 2021. Cytotoxicity and apoptosis response of hexagonal zinc oxide nanorods against human hepatocellular liver carcinoma cell line. J. King Saud Univ.-Sci. 33 (8), 101658.
Asher, N.G., Golwalkar, K.R., 2013. A Practical Guide to the Manufacture of Sulphuric Acid, Oleums, and Sulfonating Agents. Springer International Publishing, Switzerland.
Aureliano, M., Gândara, R.M.C., 2005. Decavanadate effects in biological systems. J. Inorg. Biochem. 99, 979–985.
Calderon-Garcidueñas, L., Azzarelli, B., Acuna, H., 2002. Air pllution and brain damage. Toxicol. Pathol. 30, 373–389.
Dai, L., Marie-Abele, B., Koutrakis, P., 2016. Fine particles, genetic pathways, and markers of inflammation and endothelial dysfunction analysis on particulate species and sources. J. Eposure Sci. Environ. Epidemiol. 26, 415–421.
Dechaine, G.P., Gray, M.R., 2010. Chemistry and association of vanadium compounds in Heavy oil and bitumen, and implications for their selective removal. Energy Fuels 24 (5), 2795–2808.
Dey, K.K., Jha, S., Kumar, A., Gupta, G., Srivastava, A.K., Ingole, P.P., 2019. Layered vanadium oxide nanofibers as impressive electrocatalyst for hydrogen evolution reaction in acidic medium. Electrochim. Acta 312, 89–99.
Fortoul, T.I., Rojas-Lemus, M., 2007. Vanadium as an air pollutant. In: Fortoul, T.I., Avila-Costa, M.R. (Eds.) Vanadium: Its Impact on Health. Nova Science Publishers; New York: pp. 1–6 (Chapter 1).
Fortoul, T.I., Quan-Torres, A., Sánchez, I., 2002. Vanadium in ambient air: concentrations in lung tissue from autopsies of Mexico City residents in the 1960s and 1990s. Arch. Environ. Health 57, 446–449.
Gallardo-Vera, F., Diaz, D., Tapia-Rodriguez, M., van der Goes, T.F., Masso, F., Rendon-Huerta, E., Montano, L.F., 2016. Vanadium pentoxide prevents NK-92MI cell proliferation and IFNγ secretion through sustained JAK3 phosphorylation. J. Immunotoxicol. 13 (1), 27–37.
Gallardo-Vera, F., Tapia-Rodriguez, M., Diaz, D., Fortoul van der Goes, T., Montaño, L. F., Rendón-Huerta, E.P., 2018. Vanadium pentoxide increased PTEN and decreased SHP1 expression in NK-92MI cells, affecting PI3K-AKT-mTOR and Ras-MAPK pathways. J. Immunotoxicol. 15, 1–11.
Gill, P., Moghadam, T.T., Ranjbar, B., 2010. Differential scanning calorimetry techniques: applications in biology and nanoscience. J. Biomol. Tech. 21 (4), 167–193.
Govindarajan, D., Shankar, V.M., Gopalakrishnan, R., 2019. Supercapacitor behavior and characterization of RGO anchored V2O5 nanorods. J. Mater. Sci: Mater. Electron. 30, 16142–16155.
Gutierrez-Castillo, M.E., Roubicek, D.A., Cebrian-García, M.E., et al., 2006. Effect of chemical composition on the induction of DNA damage by urban airborne particulate matter. Environ. Mol. Mutagen. 47, 199–211.
Imtiaz, M., Rizwan, M.S., Xiong, S., Li, H., Ashraf, M., Shahzad, S.M., Shahzad, M., Rizwan, M., Tu, S., 2015. Vanadium, recent advancements and research prospect: a review. Environ. Int. 80, 79–88.
Lagneborg, R., Siwecki, T., Zajac, S., Hutchinson, B., 1999. The role of vanadium in micro alloyed steel, scandinavian. J. Metallurgy. 28, 186–241.
Montiel-Dávalos, A., Gonzalez-Villava, A., Rodriguez-Lara, V., Montaño, L.F., Fortoul, T.I., López-Marure, R., 2012. Vanadium pentoxide induces activation and death of endothelial cells. J. Appl. Toxicol. 32 (1), 26–33.
Mosmann, T., 1983. Rapid colorimetric assay for cellular growth and survival: Application to proliferation and cytotoxicity assays. J. Immunol. Methods 65 (1–2), 55–63.
Nriagu, J.O., 1998. Part 2: Health Effects. John Wiley and Sons; New York: Vanadium in the environment.
Ress, N.B., Chou, B.J., Renne, R.A., Dill, J.A., Miller, R.A., Roycroft, J.H., Hailey, J.R., Haseman, J.K., Bucher, J.R., 2003. Carcinogenicity of inhaled vanadium pentoxide in F344/N rats and B6C3F1 mice. Toxicol. Sci. 74, 287–296.
Tedder, J.M., Nechvatal, A., Tubb, A.H., 1975. In: Basic Organic Chemistry: Part 5, Industrial Products. John Wiley and Sons, Chichester, UK, p. 569.
Tracey, A.S., Willsky, G.R., Takeuchi, E.S., 2007. Vanadium: Chemistry, Biochemistry, Pharmacological, and Practical Applications. CRC Press, Taylor and Francis Group.
Veiga, C., Davim, J.P., Loureiro, A.J.R., 2012. Properties and applications of titanium alloys: a brief review. Rev. Adv. Mater. Sci. 32, 133–148.
Vijayakumar, Y., Mani, G.K., Reddy, M.V.R., Rayappan, J.B.B., 2015. Nanostructured flower like V_2O_5 thin films and its room temperature sensing characteristics. Ceram. Int. 41 (2 Part A), 2221–2227.

Wahab, R., Khan, F., Kaushik, N., Kaushik, N.K., Nguyen, L.N., Choi, E.H., Siddiqui, M. A., Farshori, N.N., Saquib, Q., Ahmad, J., Al-Khedhairy, A.A., 2022a. L-cysteine embedded core-shell ZnO microspheres composed of nanoclusters enhances anticancer activity against liver and breast cancer cells. Toxicol. In Vitro 85, 105460.

Wahab, R., Khan, F., Ahmad, J., Al-Khedhairy, A.A., 2022b. Cytotoxic and molecular assessment with copper and iron nanocomposite, act as a soft eradicator against cancer cells. J. King Saud Univ.-Sci. 34 (3), 101908.

Zhang, Z., Huang, C., Li, J., 2001. Vanadate-induced cell growth regulation and the role of reactive oxygen species. Arch. Biochem. Biophys. 92, 311–320.

Zhang, R., Pan, X., Huang, Z., Weber, G.F., Zhang, G., 2011. Osteopontin enhances the expression and activity of MMP-2 via the SDF-1/CXCR4 axis in hepatocellular carcinoma cell lines. PLoS One 6 (8), e23831.